Available online at www.sciencedirect.com
SCIENCE DIRECT®
Estuarine, Coastal and Shelf Science 62 (2005) 291–300
ESTUARINE COASTAL AND SHELF SCIENCE
www.elsevier.com/locate/ECSS

Tidal and longshore sediment transport associated to a coastal structure

Diana G. Cuadrado[a,b,*], Eduardo A. Gómez[a], S. Susana Ginsberg[a]

[a]*Instituto Argentino de Oceanografía, CONICET, CC 804, 8000 Bahía Blanca, Argentina*
[b]*Dto. Geología, Universidad Nacional del Sur, San Juan 670, 8000 Bahía Blanca, Argentina*

Received 10 December 2002; accepted 10 September 2004

Abstract

In order to understand the subtidal marine dynamics relative to the coastal engineering works in the Bahía Blanca Estuary (Argentina), the balance of sediment transport caused by tidal currents was estimated in the Puerto Rosales area and compared with the predicted potential littoral transport. The breaking wave height used in the littoral drift calculation was estimated after applying different wave transforming procedures over the deepwater wave which was predicted by the occurrence of predominant wind, blowing long enough in an essentially constant direction over a fetch. The effect of a breakwater on currents and circulation was studied by bathymetric and side-scan sonar records, sedimentology, and tidal current measurements. Different modes of transport occur on either sides of the breakwater. On the east side, longshore transport is the principal mode, and on the west side, tidal transport is predominant.

Keywords: estuarine dynamic; side-scan sonar records; subaqueous dune field; fetch; wind data; Bahía Blanca Estuary (Argentina)

1. Introduction

An understanding of estuarine-harbour interrelationships in urbanised estuaries is of particular importance in the management of channel stability. Man-made modifications in coastal zones can alter the inlet geometry and hydrodynamic regime inducing changes in the environment. Coastal engineering, harbour structures and dredging modify the sediment dynamics in such a way that the maintenance of the facilities could soon become uneconomical. Hence, studies should be focused to forecast undesirable consequences like those applied in the Mediterranean (Stanley and Warne, 1993; Frihy, 2001) and North American coasts (Leatherman, 1991; Seabergh et al., 2003).

The management of harbour development, shore protection, and ecosystem conservation will require a more focused attention in the future. Because of their complexity, perceptions can often be prejudiced, and because the subject matters of engineering, management, economics, and political disciplines are not closely connected, creative solutions must be sought for the multifaceted problems of the coastal zone.

The present research was undertaken in an effort to better understand a coastal subtidal marine dynamics related to marine engineering works. The aim is to determine how a coastal structure can alter the dynamics of the zone. The study includes the estimation of the tidal and littoral transport in the area. This

* Corresponding author.
E-mail addresses: cuadrado@criba.edu.ar (D.G. Cuadrado), gmgomez@criba.edu.ar (E.A. Gómez), ginsberg@criba.edu.ar (S.S. Ginsberg).

0272-7714/$ - see front matter © 2004 Elsevier Ltd. All rights reserved.
doi:10.1016/j.ecss.2004.09.010

knowledge may also propose new ways of taking advantage of the misused natural potential of the Puerto Rosales area as a port.

2. Study area

The mesotidal Bahía Blanca Estuary (Argentina) (Fig. 1) comprises 3000 km^2 of a very complex system of channels that cross large islands and tidal flats. The interaction among tidal currents, winds and sediments present an intricate environment in continual evolution. One of the most important deep-water port systems of Argentina is located on the northern coast of this estuary. Because of its location, in the southwest of the Buenos Aires province, most of the agricultural and cattle products originating in the south of the country are traded through it. However, some navigational depths at the system access channel and mooring sites require periodic dredging.

Perillo and Piccolo (1991) found that the Bahía Blanca estuary behaves hypersynchronous as tidal range and tidal current amplitude increase headward. The mean tidal amplitude in the study area is 2.8–3.0 m (Nedeco-Arconsult, 1983). Tidal currents are reversible with maximum velocities measured at the surface of about 1.3 m s^{-1} and maximum vertically averaged values of 1.2 and 1.05 m s^{-1} for ebb and flood conditions, respectively. There are only two small fresh-water sources, which provide an annual mean runoff of 1.9 and 0.8 m^3 s^{-1}, respectively (Perillo et al., 1987). The typical mean suspended matter of 50 mg l^{-1} in surficial water (Cuadrado et al., 1994) does not vary seasonally.

Puerto Rosales is one of the harbours of the Bahía Blanca port system. It is located on the outer sector of the Principal Channel (Fig. 1), so it is affected both by inner estuarine processes such as tidal currents, and by southern storm waves. The harbour mooring sites are connected through an access channel to the Principal Channel, which has a natural maximum depth of 20 m. A 200 m stone shore-connected breakwater (see Fig. 1) was originally built one century ago to protect the western area from southward incoming waves. The whole construction was planned as the largest harbour of the region (Melo et al., 1997). However, as soon it was begun, it was abandoned due to World War I, thus modifying the original scheme of adapting the eastern side of the breakwater for ship anchorage.

To the east of the access channel lies a 100-m-wide intertidal area formed by a wide sandy tidal flat with a high content of fine material. The processes involved in this area induce high sedimentation in the harbour access channel and in mooring sites, inhibiting the navigation of large vessels. At present, the harbour provides services for small fishing ships only. The siltation in the area has been studied earlier (Gómez et al., 1994, 1997; Cuadrado et al., 1996, 2000; Federici

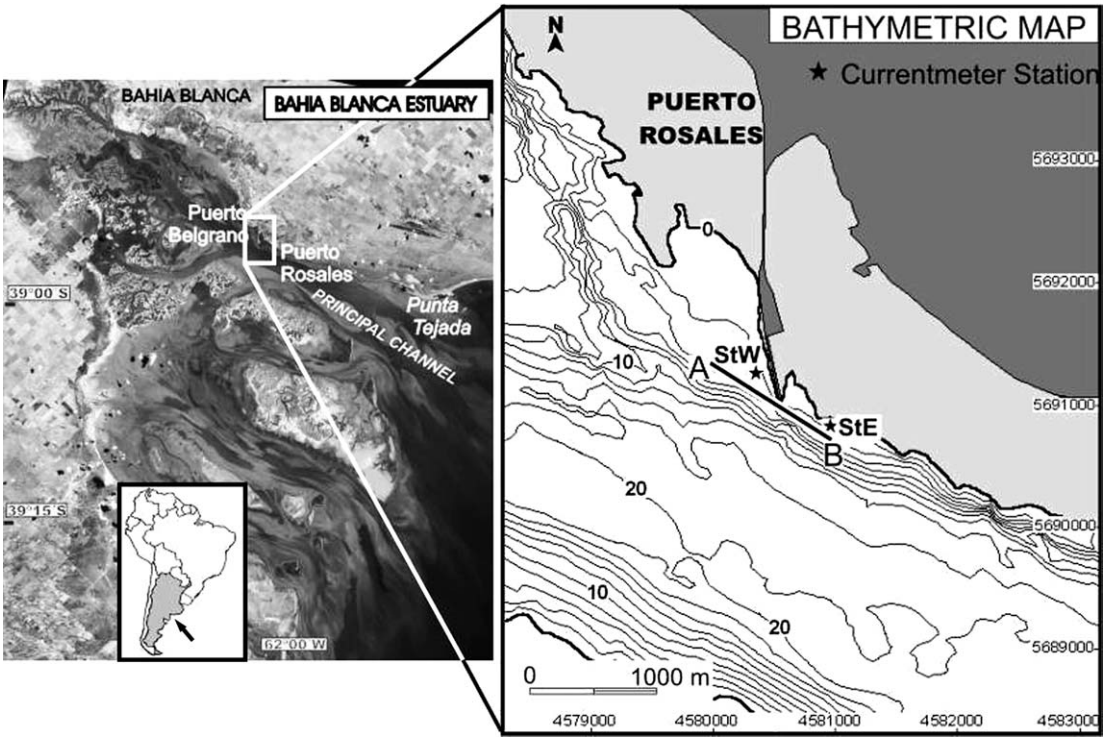

Fig. 1. Location of the study area at Bahía Blanca Estuary, Argentina. The coordinates in the bathymetric map are in Gauss Krüger projection and the depths in meters. The intertidal zone is shaded.

et al., 2001). Despite the advantageous location that enables vessels to save 20 km when accessing the harbour, Puerto Rosales has not been operative for long periods of time (Melo et al., 1997).

Because of the geographical situation of Puerto Rosales, the maritime climate in the area is composed by locally generated wind waves and by the swell that enters through the estuary mouth. In the Puerto Rosales area the locally generated wind waves are short wavelengths with periods from 2 to 4 s. Offshore, the period of the swell can reach values of 7 to 8 s. The most frequent swell comes from the south with significant wave heights (Hs) between 1 and 1.9 m with associated periods (T) from 8 to 10 s (Nedeco-Arconsult, 1983).

In the surrounding area east of Puerto Rosales, the coast (supratidal area) is covered mainly by Holocene vegetated dune belts and by a small mobile dune field. Most of the dune belts are vegetated due to a notable increment of the mean yearly rainfalls since the middle of last century (Melo and Zinger, 1997). The major feature on the coast is the formation of a sand spit at Punta Tejada (Fig. 1).

3. Methodology

Geomorphological characteristics were defined by performing bathymetric and side-scan sonar surveys. Bathymetric profiles were taken using a 308 kHz Raytheon echosounder and an EG&G SMS 960 side-scan sonar operating at 105 kHz with a pulse length of 0.1 ms. In all the survey runs, the side-scan sonar was set to a 100 m range. While the echosounder gives a vertical profile of depth, the side-scan sonar builds a vertical projection of seabed characteristics by differences in the intensity of the returning acoustic signals, covering a 200-m-wide area. The areas of shadows or low backscattering strength appear as light tones, whereas high backscattering strength is indicated by darker tones.

The vessel position during profiling was determined by a real time Satloc GPS operating in differential mode with a maximum error of 3 m. The record depths were reduced with the continuous tidal records from Puerto Belgrano tidal gauge. All maps were made using a Gauss–Krüger projection. The bathymetry is presented in Fig. 1.

Twenty-six bottom sediment samples were collected at the portion of the Principal Channel close to Puerto Rosales using a Shipek grab sampler. Samples were taken whenever changes in morphology occurred. They were processed following standard laboratory procedures for grain-size analysis to determine the mean grain size, sorting and skewness (Folk, 1974).

In order to analyse current behaviour, tidal currents were continuously recorded at a frequency of 0.5 Hz during two tidal cycles by deploying fifteen InterOcean current-meters (model 135). All the current-meters were located 1 m above the bottom where the depth was 7 m.

The wind data were provided by a meteorological station placed in Puerto Rosales. The records had a 30 min sampling period and a time series of 13 months was used in a statistical study in order to analyse the contribution of winds on the transport parallel to the coast. These data were used to predict the wave parameters, since the only wave-gauge in the area is located far from the mouth of the Bahía Blanca estuary. Therefore, the waves (sea and swell) were inferred from the recorded wind data by using nomograms and expressions from USACE (2002).

4. Results

The strong difference between the zones located at both sides of the breakwater of Puerto Rosales can be observed in Fig. 1. On the west side of the breakwater (WS), the 2 m isobath runs parallel to the structure for about 500 m and then it separates perpendicularly. The characteristic slope on the WS for depths between 0 and 4 m is 0.4%, increasing to 2.8% for depths between 4 and 18 m. On the east side of the breakwater (ES) the zero isobath, extends from the end of the structure straight away to the ESE after running through the access channel. Thus a wide tidal plain to the north is exposed at low tide, followed by a steep slope (3.2%) from 0 to 16 m depth towards the central portion of the Principal Channel.

The spatial distribution of different grain size classes has been mapped showing differences between ES and WS areas (Fig. 2). Fine sand is present in the channel sides on the ES (mean grain size between 2.79 and 2.44 Ø); while in the tidal flats the grain size is finer than 3 Ø, reaching values of coarse silt (4–5 Ø). The sediments are coarser on the WS, with medium sand near the breakwater at 3 m depth. Mean grain size here is between 2.71 and 1.73 Ø. The upper tidal flat is formed by silt (4.19 Ø). Some coarse, mean grain-size samples have up to 12% shells, giving a typical poorly sorted distribution with a negative skewness. The coarser sediment (medium sand) is found at a depth of 17–18 m.

The side-scan sonar record obtained at ES along the 4 m isobath (Fig. 3) reveals a field of asymmetrical medium 2D dunes according to Ashley's classification (Ashley, 1990). The sediment here is fine sand ($D_{50}=2.6$ Ø). The medium dunes are aligned in a N–S direction with a spacing of 8–18 m and less than 0.8 m height. Their lee side oriented westward indicates a net sand transport into the estuary, contrary to what occurs in the central portion of the channel (Cuadrado et al., 2001). At WS the dune field abruptly ends, forming a 3.5 m step as can be observed in the echosounder record

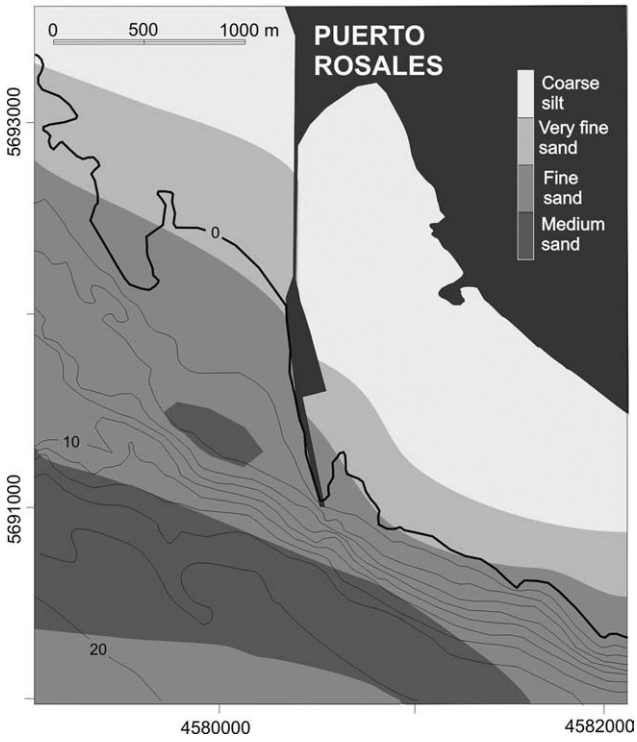

Fig. 2. Grain size distribution of superficial sediment samples obtained in the study area.

(Fig. 3). West of the dune field, the sonograph shows a bottom with a relatively high backscattering strength (darker grey background) along 110 m. Beyond this area, the bottom is covered by loose sand forming small dunes (0.4 m maximum height, 5 m average spacing) of variable orientation.

Because no annual variation was detected in the current measurements (Nedeco-Arconsult, 1983), only two records from current-meters simultaneously deployed during two tidal cycles in spring were used in order to compare the current behaviour and to compute its ability to transport sediment as bed-load. They were located at two stations, StE and StW, in the ES and WS of the breakwater, respectively (see Fig. 1). Representative plots of the intensity and direction of the currents in the area are shown in Fig. 4. The tidal behaviour reveals an important spread of the mean values in current velocity and direction. Ebb and flood tidal current directions were nearly opposite. Current mean direction at StE changed from 110° (for the ebb) to 300° (for the flood), while at StW, it changed from 150° to 300°. The velocity was slightly higher in StW than in StE. Maximum currents in StW were 0.75 m s^{-1} and 0.60 m s^{-1} during ebb and flood, respectively (Fig. 4a). At StW the duration of both hemicycles was almost the same (about 6 h each).

Ebb currents are quite different from flood ones on the ES (Fig. 4b). The ebb lasted nearly 5 h, with the highest intensities (up to 0.45 m s^{-1}) in the first 2 h of the hemicycle. From this moment, current speed progressively dropped to values between 0.05 to 0.15 m s^{-1}, maintaining the intensity during the last 3 h of the ebb hemicycle. The flood lasted more than the ebb (7 h) with its maximum intensity (0.30–0.40 m s^{-1}) reached 1.5 h from the beginning of the cycle, being almost constant for 4.5 h, and decreasing during the last hour of the flood hemicycle.

The two stations behave differently. While in StW the current speed is greater than the critical velocity (threshold velocity for the initiation of bed-load transport) in both ebb and flood tides, in StE the current speed only surpasses the critical velocity during the ebb tide for a short time.

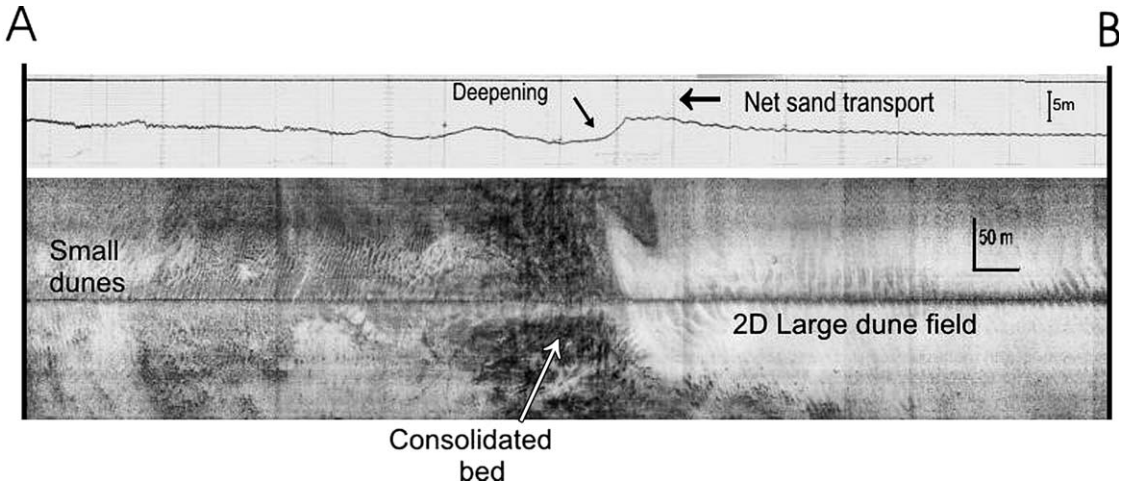

Fig. 3. Side scan sonar sonograph (below) and echo sounder record (above) registered along the A–B profile during high tide (location shown in Fig. 1).

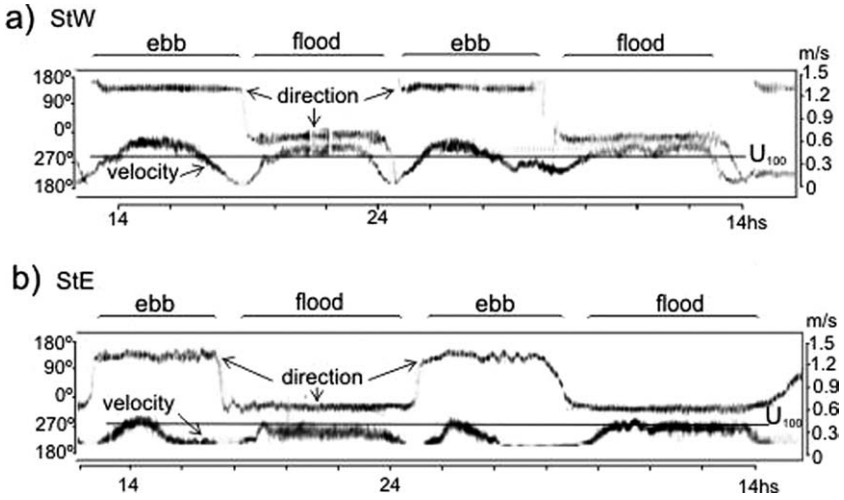

Fig. 4. Currentmeter records for (a) Station StW and (b) Station StE, corresponding to two consecutive tidal cycles, showing the progress of the tidal current direction and velocity. The left scale corresponds to the current direction and the right scale to the current velocity. U_{100c} was drawn to show the velocity exceeding that value.

5. Discussion

In order to evaluate the capability of tidal currents to transport sediment, the potential sediment transport rate was computed using the Bagnold's model (Bagnold, 1966) modified by Gadd et al. (1978) as:

$$Q_t = \beta(U_{100} - U_{100c})^3 \quad (1)$$

where U_{100} is the velocity of the current and U_{100c} is the critical velocity, both at 1 m above the bottom. Despite the simplicity of this model, it fits the observations very well (Gómez, 1992). β is an empirical value equal to 1.73×10^{-5} g s^2 cm^{-4}, constant for different grain sizes (Gómez, 1992; Amos et al., 1993; and Li and Amos, 1993). In order to compute U_{100c}, the D_{50} of the sediment was obtained from the grain size analysis of bottom samples taken at the current-meter stations. U_{100c} was calculated from the modified Shield's curve (Madsen and Grant, 1976).

Since the rate of sediment transport is a function of the third power of the excess in tidal current velocity, the mean sediment transport rate computed from the mean current speed alone usually underestimates its value in a quantity related to the standard deviation of the data. However, from the scatter plot of the current data, it is possible to obtain the maximum (U_{max}), mean (U_{mean}) and minimum current speed (U_{min}). For a given period of time it is possible to obtain a good approximation of the mean potential sediment transport rate (Q_{mean}) considering the following weighted average:

$$Q_{mean} = (Q(U_{max}) + Q(U_{min}) + 2Q(U_{mean}))/4 \quad (2)$$

The D_{50} of the sediments located at ES was 2.79 Ø, resulting in $U_{100c} = 0.3752$ m s^{-1}. The unconsolidated sediments at WS were coarser with a D_{50} of 1.95 Ø and $U_{100c} = 0.3959$ m s^{-1}. The sediment transport estimation was made when tidal current speeds exceeded the corresponding critical values. As tidal currents are practically opposite each other, the net sediment transport rates were obtained subtracting the total ebb from the total flood transport. Considering that these are characteristic values for the area, the transported potential mass was extrapolated to a whole year and its volume estimated by assuming a sediment density of 2.65 kg m^{-3} (Table 1).

The dark background identified in the sonograph along a stretch of 110 m at WS (Fig. 3) reveals a total absence of loose materials, showing a bottom composed of lithified materials partially covered by sand patches. This fact would be related with the high net tidal transport in the WS taking into account that the direction of transport is nearly orthogonal to the 110 m stretch that is free of loose sediment. The calculated amount of sediment (18.98 m^3 m^{-1} yr^{-1}, Table 1), multiplied by the sand-free width (110 m) gives a maximum value of 2.1×10^3 m^3 yr^{-1} of sand that could be transported by the tidal currents. In order to get a hard bottom out of loose sediment, this amount of sand would have had to be blown away by the residual ebb currents. The sand would be transported towards the deeper parts of the Principal Channel feeding the subaqueous dunes characterised by a seaward direction (Cuadrado et al., 2003).

On the other hand, the presence of the subaqueous dune field with an inward orientation at ES and N 110° direction cannot be explained by the small magnitude of

Table 1
Sediment transported as bed load by tidal currents at stations StW and StE over two tidal cycles

Station	Cycle I		Cycle II		Balance		Net transport direction
	Ebb (kg m^{-1})	Flood (kg m^{-1})	Ebb (kg m^{-1})	Flood (kg m^{-1})	kg m^{-1} yr^{-1}	m^3 m^{-1} yr^{-1}	
StE	−0.024	0.000	−0.109	0.0159	−39.758	−0.015	N 110°
StW	−154.181	29.147	−61.5978	39.240	−50304.77	−18.983	N 150°

Negative numbers indicate net erosion.

the sediment transport rate computed from the tidal currents (1.5×10^{-2} m^3 m^{-1} yr^{-1}). Therefore, another explanation must be found for its presence.

The analysis of the wind data shows that the predominant directions are NW, NNW and SE with a velocity range between 5 and 10 m s^{-1}. While the ES is sheltered from WNW winds due to the presence of the breakwater, winds from the SW quadrant have a short fetch up to 6 km long. The wind rose is shown in Fig. 5. The SE winds have the longest fetch for the Puerto Rosales area, reaching 13 km from the harbour to the sand banks located at the estuary entrance (Cuadrado and Perillo, 1997a,b). Hence, the winds from the SE were chosen as those that can generate the most significant wind waves reaching the Puerto Rosales area.

Considering the role of winds in wave generation, the significant wave height and period over a fetch may be estimated when wind speed, fetch length and duration of wind over a fetch are given. The basic tenet of the empirical prediction method is that interrelationships among dimensionless wave parameters are governed by universal laws. Perhaps the most important of these laws is the fetch-growth law (Resio et al., 2002). Given a constant wind speed and direction over a fixed fetch, it is expected that waves will reach a stationary fetch-limited state of development. So, on the basis of a complete wind duration record over a year, a deepwater wave forecast was performed as a function of wind speed, fetch length, and wind duration. The duration required to achieve fetch-limited conditions is a function of wind speed. Thus, the predominant wind speeds (10 m s^{-1} and 15 m s^{-1}) over a fetch of 13 km were considered to obtain a steady-state condition.

Hence, deepwater wave parameters were forecasted outside the estuary as a function of the predominant SE wind speeds, fetch length, and wind duration (Table 2). After different procedures for transforming waves from offshore to nearshore, a calculated breaker height was obtained on the Puerto Rosales coast. The littoral sediment transport Q_w attained for these waves was based on the relationship of sediment transport and studied by Komar and Inman (1970) (see Appendix A). The angle between the shore and the direction of the wave crest at breaking (α_b), was considered as 70° at

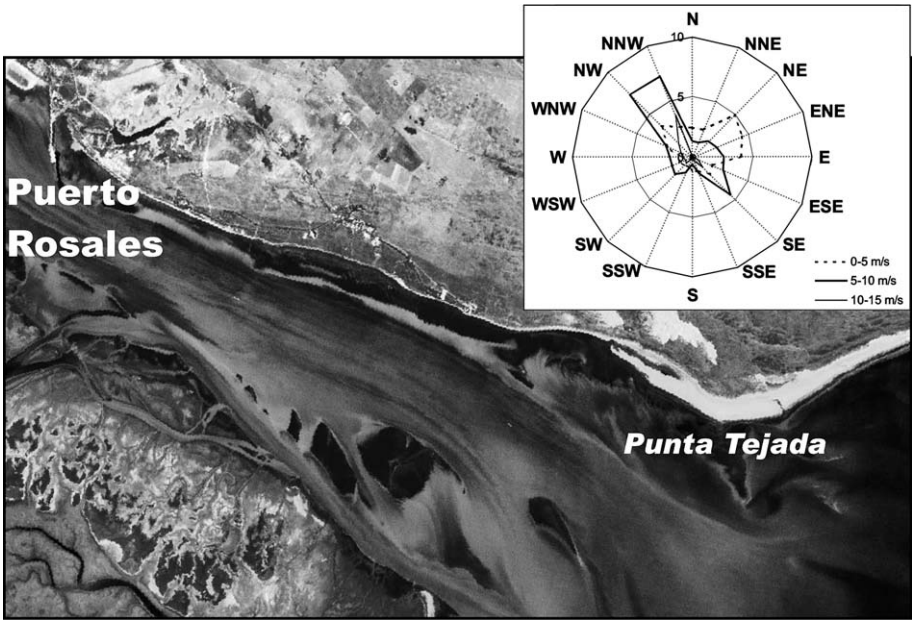

Fig. 5. Annual wind rose superposed on the coast of the Bahía Blanca Estuary. Note the relative greatest magnitude of the SE fetch which allows the formation of the most important local waves within the estuary.

Table 2
Results of the annual wind analysis for the SE wind direction and the total potential sediment transported by longshore currents

Wind velocity	Wind statistical study	Potential longshore sediment transport calculation				
	Duration (h)	Frequency	H_0 (m)	T (s)	Q_w (m^3 yr^{-1})	Total (m^3 yr^{-1})
5–10 m s^{-1}	2	8	0.4	2	85.79	11777
	2.5	6	0.5	2.2	184.20	
	3	5	0.51	2.3	240.60	
	3.5	6	0.6	2.3	388.50	
	4	6	0.6	2.3	444.01	
	4.5	11	0.6	2.3	499.51	
	5	5	0.6	2.3	555.01	
	5.5	6	0.6	2.3	610.51	
	6	6	0.6	2.3	666.01	
	6.5	5	0.6	2.3	721.51	
	7	2	0.6	2.3	777.01	
	7.5	1	0.6	2.3	832.51	
	8	1	0.6	2.3	888.01	
	8.5	1	0.6	2.3	943.51	
	9	1	0.6	2.3	999.01	
	12.5	1	0.6	2.3	1387.52	
	14	1	0.6	2.3	1554.02	
10–5 m s^{-1}	1.5	1	0.6	2.3	166.50	24057
	2	1	0.7	2.7	354.71	
	3	1	1	3	1206.98	
	4	1	1	3	1609.30	
	4.5	1	1	3	1810.46	
	5	1	1	3	2011.63	
	5.5	1	1	3	2212.79	
	6	1	1	3	2413.95	
	6.5	2	1	3	2615.11	
	7.5	1	1	3	3017.44	
	8	2	1	3	3218.60	
	8.5	1	1	3	3419.76	

H_0, deepwater wave height; T, wave period obtained from USACE nomograms.

Puerto Rosales. The K parameter has recently been determined empirically by del Valle et al. (1993) and it is correlated with the median sediment grain size:

$$K = 1.4e^{(-2.5D_{50})} \quad (3)$$

As $D_{50} = 2.79$ Ø, $K = 0.96$, quite close to the unity. The breaker index (k), which is a function of the beach slope (Weggel, 1972) is regarded as 1.0.

The potential longshore sediment annually transported is obtained multiplying the Q_w values by the annual wind frequency, which originates the predicted waves (Table 2). Thus, the annual net sediment transport obtained for the most frequent wind velocity (5 to 15 m s^{-1}) was estimated as nearly 3.6×10^4 m^3 yr^{-1}. For wind speed between 10 to 15 m s^{-1}, the estimated transport (2.4×10^4 m^3 yr^{-1}) is much greater than for lower wind speeds (1.1×10^4 m^3 yr^{-1}) although this occur more often and last longer.

To compare the results of predicted longshore sediment transport (3.6×10^4 m^3 yr^{-1}) with those obtained from tidal currents (1.5×10^{-2} m^3 m^{-1} yr^{-1}) measured on the ES, both measures must be given in the same magnitude. As tidal current sediment transport was computed per unit of width, a simple calculation indicates that it must work through a width of 2.4×10^3 km in order to counterbalance the potential amount of sediments transported by longshore currents. Hence, it is possible to assert that the amount of sediment transported by tidal currents is irrelevant compared to the north-westward littoral drift. Thus, the presence of the subaqueous dune field with the inward estuary direction of migration should be mainly the consequence of locally generated waves entering the estuary.

The breakwater exerts an important action on the dynamics of the area. The current characteristics are different on both sides. When maximum velocities were reached on the WS at mid ebb cycle, current velocities on the ES dropped sharply. Such behaviour may be related to a hydraulic protection, since the breakwater may produce a flux separation with a relatively calm zone on the ES.

An additional effect that the breakwater has on the dynamics of the zone is related to the interruption of the dune field which migrate to the inner estuary. Consequently, the amount of available sand transported by longshore currents should not be greater than the estimated sediment removed by tidal currents at WS (2.1×10^3 m^3 yr^{-1}). However, this value is much smaller than the large predicted transport by longshore currents (Table 2). This means that there is a lesser amount of sediment carried by these currents than the transporting capability of the littoral drift.

To identify the source of sediments that feed the littoral transport, the northern coast of the outer Bahía Blanca estuary must be considered. The presence of a shoreline attached sand spit at Punta Tejada (18 km east of Puerto Rosales, Fig. 5), is strong evidence of the existence of an inward estuary wave powered transport of sand. The origin of these sediments would be the mobile dune field that has been largely vegetated during the last century as a result of an increased mean annual precipitation. This increase caused the decrease of the area covered by mobile dunes, reducing the sand sources which supply the north-eastern beaches in the Punta Tejada zone by the action of the NW prevailing winds. This is most likely the reason why there is a smaller mobile sediment supply at present than in the past.

6. Conclusions

Due to the shore-connected breakwater, both sides of Puerto Rosales behave in a different manner. The present study confirmed the different modes of transport at both sides of the breakwater. While the longshore transport is the principal mode on the east side of the

breakwater, the tidal transport is predominant on the west side, producing the interruption of the littoral drift. Tidal currents are slightly stronger on the west side than on the east side, removing the loose sediment transported by longshore currents almost completely, thus exposing a consolidated and lithified bottom.

Considering that tidal currents at the west side of the breakwater are able to transport 2.1×10^3 $m^3\,yr^{-1}$ of sediment, and that the westward littoral drift is stopped by these currents, the littoral drift is not greater than this bulk. Moreover, this quantity of sediment is lesser than the transporting capability of the littoral drift, which implies that the vegetation of the mobile dunes located northeast of Puerto Rosales, retains the loose sediment.

The subaqueous dune field whose orientation indicates sediment movement into the estuary evidences the westward longshore transport at 4 m depth. This field would be related to the shoreline attached sand spit present 18 km east of Puerto Rosales. The origin of this feature would be the mobile dune field present on the coast, which is suffering a decrease in the supply of sediment because of the present vegetation of the coastal dunes. This is why there is low longshore sediment transport compared to the budget that the longshore currents are able to transport.

The hydrodynamical characteristics due to the presence of the stone breakwater would be useful for harbor interests. Contrary to what occurs on the east harbor side, bathymetry, sediment, and the ability of tidal currents to transport sediment indicate that the area located to the west of the stone breakwater is free of siltation. These facts open up the possibility of dredging this area with minimum maintenance. In addition, should a suitable current-transparent pier be constructed, even larger ships, than those currently operating in Puerto Rosales could use the port facilities.

7. List of special characters

D_{50}	median grain size
U_{100}	current velocity at 100 cm above the bottom
U_{100c}	critical velocity at 100 cm above the bottom
X	straight line fetch distance over which the wind blows
H_{m_0}	energy-based significant wave height
T	wave period
u_*	friction wind velocity
g	gravity acceleration
ρ	mass density of water
ρ_s	mass density of sediment
k	breaker index
n	in-place sediment porosity
H_b	height wave at breaking
H_0	deepwater wave height
α	angle between the shore and the direction of the wave crest
Ω_b	breaker height index
L_0	deepwater wave length
K_r	refraction coefficient
C_0	wave celerity in deepwater
C_1	wave celerity at location 1

Acknowledgements

Funding for this study was provided by APCyT (PICT 98 07-03955); SGCyT UNS (PGI 24/ZH08) and CONICET (PEI N°6025–PIP N°2611). The authors would like to express their gratitude for the assistance of Roberto Zibechi, Carlos Galán, Luis Kaufman, and the crew of RV Buen Día Señor during the fieldwork. We appreciate the collaboration in the laboratory works of Hugo Pellegrini and Miguel Colombani. We thank Dr Jose J. Alonso del Rosario for his critical readings and comments.

Appendix A. Deepwater wave transformation and longshore sediment transport calculation

Based on different procedures mentioned in USACE (2002) for transforming waves, the breaker wave is calculated from its offshore generation up to the surf zone approach. The longshore sediment transport is then obtained.

In the first place, based on complete wind duration records, the prediction of deepwater waves from nomograms was obtained. The governing equations for the wave growth under limited fetch conditions when a wind blows for sufficient time (t_m) to achieve steady state (Resio et al., 2002) are:

$$\frac{gH_{m_0}}{u_*^2}=4.13\times10^{-2}\left(\frac{gX}{u_*^2}\right)^{1/2} \tag{A1}$$

for wave height, and

$$\frac{gT}{u_*}=\frac{1}{2.727}\left(\frac{gX}{u_*^2}\right)^{1/3} \tag{A2}$$

for the period, where X is the straight-line fetch in meters, H_{m_0} is the significant wave height in meters, T is the wave period is seconds, u_* is the friction wind velocity and g is the acceleration due to the gravity. Resio and Vincent (1979) suggested that the wave conditions in fetch areas are actually relatively insensitive to its width, so a straight-line fetch is used to define the fetch length.

The duration required to achieve fetch-limited condition (t_m) is a function of wind speed (Resio and Vincent, 1979). In the present study, considering a fetch of 13 km, the steady-state condition was reached with a duration of 3.3 h for a wind speed of 10 m s^{-1}, and 3 h for a wind speed of 15 m s^{-1}. For duration less than t_m the wave characteristics had to be calculated for each one. Once the t_m is reached the wave characteristics do not depend on the length of time the wind blows.

Expressions (A1) and (A2) were used when the wind duration exceeded the t_m, and expression (A3) was used when the duration was less:

$$\frac{gX}{u_*^2}=5.23\times10^{-3}\left(\frac{gt}{u_*}\right)^{3/2} \tag{A3}$$

where t is the wind duration.

When a wave propagates into a region where the depth is variable, the changes in wave speed change the direction of wave travel and change the amplitude of the wave. Therefore, the refraction and shoaling must be considered. Following the procedures for transforming waves from offshore to nearshore locations used by Vincent et al. (2002), the refraction coefficient is estimated as:

$$K_r=\left(\frac{1-\sin^2\theta_0}{1-\sin^2\theta_1}\right)^{1/4} \tag{A4}$$

where θ_0 is the angle between the shore and the direction of the wave crest at deepwater, and θ_1 is the same angle but at location 1. At location 1 the depth (d) is greater than 3 m, verifying the condition of transitional water ($d/L<0.5$). With this, θ_1 in eq. (A4) is computed by

$$\sin\theta_1=\frac{C_1\sin\theta_0}{C_0} \tag{A5}$$

Considering the wave parameters in deepwater (Demirbilek and Vincent, 2002), C_0 is the wave celerity in deepwater and C_1 is the celerity at location 1 is defined as

$$C_0=\frac{gT}{2\pi} \tag{A6}$$

$$C_1=\frac{L_1}{T} \tag{A7}$$

where L_1 is the wave length at location 1. This is computed using the following approximation:

$$L_1=L_0\sqrt{\tanh\left(\frac{2\pi d}{L_0}\right)} \tag{A8}$$

with an error of less than 2% with respect to the correct computation due to a trial and error solution.

The refraction coefficient is needed to obtain the equivalent unrefracted deepwater wave that can be derived from the relationship (Smith, 2002):

$$H'_0=K_rH_0 \tag{A9}$$

Finally, the breaking wave height (H_b) was derived from the breaker height index Σ_b

$$\Omega_b=\frac{H_b}{H_0} \tag{A10}$$

where H_0 is the deepwater wave height.

An estimation of Ω_b can be achieved following the derivation of Komar and Gaughan (1973) as a semi-empirical relationship from the linear wave theory

$$\Omega_b=0.56\left(\frac{H'_0}{L_0}\right)^{-\frac{1}{5}} \tag{A11}$$

where the coefficient was empirically determined from laboratory and field data. H'_0 is the equivalent unrefracted deepwater wave height, and L_0 is the deepwater wave length obtained as

$$L_0=\frac{gT^2}{2\pi} \tag{A12}$$

where T means the wave period.

Using the estimated wave breaker, the sediment transport was computed from the USACE formula for littoral sand transport (Rosati et al., 2002):

$$Q_w=K\left(\frac{\rho\sqrt{g}}{16k^{1/2}(\rho_s-\rho)(1-n)}\right)H_b^{5/2}\sin(2\alpha_b) \tag{A13}$$

where ρ is the density of water, ρ_s is the density of sediment, K is the breaker index, n is the sediment porosity with a computed value of 0.4, H_b is the wave height at breaking and α_b is the angle between the shore and the direction of the wave crest at breaking.

References

Ashley, G., 1990. Classification of large-scale subaqueous bedforms: a new look at an old problem. Journal of Sedimentary Petrology 60, 160–172.

Amos, C.L., Gómez, E.A., Li, M.Z., 1993. Sand transport — measurements and predictions. Proceedings Euromech 310, Le Havre, France.

Bagnold, R.A., 1966. An approach to the sediment transport problem from general physics. Physiographic and Hydraulic Studies of Rivers. Geological Survey Professional paper 422-1, U.S. Governmental Printing Office, 36 pp.

Cuadrado, D.G., Perillo, G.M.E., Marcos, A., 1994. Análisis preliminar del transporte del sedimento en suspensión en Puerto Rosales. Actas V Reunión Argentina de Sedimentología, 229–234.

Cuadrado, D.G., Melo, W., Gómez, E.A., 1996. Evolución de la Tasa de Sedimentación en Puerto Rosales, Estuario de Bahía Blanca. Actas VI Reunión Argentina de Sedimentología, 261–266.

Cuadrado, D.G., Perillo, G.M., 1997a. Migration of intertidal sandbanks, Bahía Blanca Estuary, Argentina. Journal of Coastal Research 13 (1), 139–147.

Cuadrado, D.G., Perillo, G.M., 1997b. Principal component analysis applied to geomorphologic evolution. Estuarine, Coastal and Shelf Science 44, 411–419.

Cuadrado, D.G., Federici, G.A., Gómez, E.A., Natali, M., 2000. Modification on Rosales Port sedimentation rate, Argentina. Profile 18, CD-ROM (13), 6 pp.

Cuadrado, D.G., Gómez, E.A., Ginsberg, S.S., 2001. Sediment transport inferred by submarine bedforms. Geoacta 26, 71–80.

Cuadrado, D.G., Gómez, E.A., Ginsberg, S.S., 2003. Large-scale transverse bedforms in a mesotidal estuary. Revista Asociación Argentina de Sedimentología 10 (2), 163–172.

del Valle, R., Medina, R., Losada, M.A., 1993. Dependence of coefficient K on grain size, Technical Note No. 3062. Journal of Waterway, Port, Coastal, and Ocean Engineering 119 (5).

Demirbilek, Z., Vincent, L., 2002. Water wave mechanics. In: Vincent, L., Demirbilek, Z. (Eds.), Coastal Engineering Manual, Part II, Coastal Hydrodynamics. Engineering Manual, 1110-2-1100. U.S. Army Corps of Engineers, Washington, DC, Chapter 1.

Federici, G.A., Gómez, E.A., Cuadrado, D.G., Natali, M., 2001. Acción de las olas en la sedimentación de Puerto Rosales, Argentina. Abstract IX Congreso Latinoamericano de Ciencias del Mar, 4 pp.

Frihy, O., 2001. The necessity of environmental impact assessment (EIA) in implementing coastal project: lessons learned from the Egyptian Mediterranean. Coastal, Ocean and Coastal Management 44, 489–516.

Folk, R.L., 1974. Petrology of Sedimentary Rocks. Hemphill, Austin, TX, 182 pp.

Gadd, P.E., Lavelle, J.W., Swift, D.J.P., 1978. Estimates of Sand Transport on the New York Shelf using Near-bottom current meter observations. Journal of Sedimentary Petrology 48 (1), 239–252.

Gómez, E.A., 1992. Analysis of sea carousel deployments from offshore Western Newfoundland and Sable Island Bank, Canada. Geological Survey of Canada, Unpublished report, 90 pp.

Gómez, E.A., Cuadrado, D.G., Melo, W.D., 1994. Posible causa de la sedimentación en Puerto Rosales. Abstracts IX Coloquio de Oceanografía, 12.

Gómez, E.A., Melo, W.D., Cuadrado, D.G., 1997. Evaluation of environmental conditions at Rosales Harbour, Bahía Blanca Estuary, Argentina. Zentralblatt für Geologie und Paläontologie 3–6, 663–670.

Komar, P.D., Gaughan, M.K., 1973. Airy wave theory and breaker height prediction. In: Proceedings of the 13th Coastal Engineering Conference, American Society of Civil Engineers, pp. 405–418.

Komar, P.D., Inman, D.L., 1970. Longshore sand transport on beaches. Journal of Geophysical Research 75, 5914–5927.

Leatherman, S.P., 1991. Coast, beaches. In: Kiersch, G.A. (Ed.), The Heritage of Engineering Geology. Centennial Special, vol. 3. Geological Society of America, Boulder, CO, pp. 183–200.

Li, M.Z., Amos C.L., 1993. SEDTRANS92: Re-evaluation and upgrade of the AGC Sediment Transport Model. Geological Survey of Canada Open File Report 2769, 115 pp.

Madsen, O.S., Grant, W.D., 1976. Quantitative description of sediment transport by waves. In: Proceedings Fifteenth International Coastal Engineering Conference, American Society of Civil Engineers, vol. 2, pp. 1093–1112.

Melo, W.D., Zinger, S., 1997. El comportamiento dinámico del arroyo Napostá Chico, Buenos Aires. Actas Primeras Jornadas Nacionales de Geografía Física, 122–129.

Melo, W.D., Cuadrado, D.G., Gómez, E.A., 1997. Importancia de las Condiciones Ambientales en la Planificación Territorial del área de Puerto Rosales. Actas Primeras Jornadas Nacionales de Geografía Física, 147–152.

Nedeco-Arconsult, 1983. Estudio de dragado al canal de acceso al Puerto de Bahía Blanca. Technical Report (3 volumes).

Perillo, G.M.E., Piccolo, M.C., 1991. Tidal response in the Bahía Blanca Estuary. Journal of Coastal Research 7, 437–449.

Perillo, G.M.E., Piccolo, M.C., Arango, J.M., Sequeira, M.E., 1987. Hidrografía y circulación del estuario de Bahía Blanca (Argentina) en condiciones de baja descarga. In: Proceeding 2° Congreso Latinoamericano de Ciencias del Mar, La Molina, II, pp. 95–104.

Resio, D.T., Vincent, C.L., 1979. A comparison of various numerical wave prediction techniques. In: Proceedings of the 11th Annual Ocean Technology Conference, Houston, TX, p. 2471.

Resio, D., Bratos, S., Thompson, E., 2002. Meteorology and wave climate. In: Vincent, L., Demirbilek, Z. (Eds.), Coastal Engineering Manual, Part II, Coastal Hydrodynamics. Engineering Manual, 1110-2-1100. U.S. Army Corps of Engineers, Washington, DC, Chapter 2.

Rosati, J., Walton, T., Bodge, K., 2002. Longshore sediment transport. In: Walton, T. (Ed.), Coastal Engineering Manual, Part III, Coastal Hydrodynamics. Engineering Manual, 1110-2-1100. U.S. Army Corps of Engineers, Washington, DC, Chapter 2.

Seabergh, W.C., Cialone, M.A., McCormick, J.W., 2003. Inlet modifications and the dynamics of Barnegat Inlet, New Jersey. Journal of Coastal Research 19 (3), 633–648.

Smith, S., 2002. Surf zone hydrodynamics. In: Vincent, L., Demirbilek, Z. (Eds.), Coastal Engineering Manual, Part II, Coastal Hydrodynamics. Engineering Manual, 1110-2-1100. U.S. Army Corps of Engineers, Washington, DC, Chapter 4.

Stanley, D.J., Warne, A.G., 1993. Nile delta: recent geological evolution and human impact. Science 260, 628–634.

USACE, 2002. Coastal Engineering Manual, 1110-2-1100. U.S. Army Corps of Engineers, Washington, DC, 6 volumes.

Vincent, L., Demirbilek, Z., Weggel, R., 2002. Estimation of nearshore waves. In: Vincent, L., Demirbilek, Z. (Eds.), Coastal Engineering Manual, Part II, Coastal Hydrodynamics. Engineering Manual, 1110-2-1100. U.S. Army Corps of Engineers, Washington, DC, Chapter 3.

Weggel, J.R., 1972. Maximum breaker height. Journal of the Waterways, Ports, and Coastal Engineering Division 98, 529–548.